Composites Part B 87 (2016) 149–160

Contents lists available at ScienceDirect

Composites Part B

journal homepage: www.elsevier.com/locate/compositesb

A simple-input method to analyze thick composite tubes under pure bending moment reinforced by carbon nanotubes

Hamidreza Yazdani Sarvestani*, Ali Naghashpour, Alireza Gorjipoor

Concordia Centre for Composites (CONCOM), Department of Mechanical and Industrial Engineering, Concordia University, Montreal, Canada H3G 1M8

ARTICLE INFO

Article history:
Received 11 March 2015
Received in revised form
27 August 2015
Accepted 16 October 2015
Available online 2 November 2015

Keywords:
A. Glass fibres
B. Strength
C. Analytical modelling
C. Finite element analysis (FEA)
D. Mechanical testing

ABSTRACT

In the present work, thick laminated carbon nanotube-reinforced composite straight tubes subjected to pure bending moments are investigated using a new simple-input analytical method. The most general displacement field of elasticity for an arbitrary laminated orthotropic tube is employed to analytically determine stresses under pure bending moments based on a layer-wise method. The accuracy of the proposed method is subsequently verified by comparing the numerical results obtained using the proposed method and finite element method (FEM) with experimental data. The results show good agreement. Also, high efficiency in terms of computational time is achieved when the proposed method is used as compared with FEM. In addition, effects of using nanotubes in laminated composites on stress distributions of orthotropic straight tubes are investigated.

1. Introduction

Composite tube structures are frequently used in aerospace applications. Therefore, prediction of the state of stress in different layers of composite tubes is of theoretical interest and practical importance. In all applications, accurate design and inclusive analysis are important to ensure safety and proper performance of composite structures. It should be noted that stress analysis of cylindrical composite structures is often a complex task. A few reasons exist for such a complexity. First, the governing equations of composite tubes are complicated. Second, a major source of intricacy is the layerwise failure of composite materials. In fact, as soon as a layer fails, a delamination happens or a crack propagates inbetween the plies, material properties degrade and sometimes the governing equations could be different. Moreover, the tube geometry is a lot more complicated than flat geometry.

The researchers have performed a lot of investigations on composite tubes under different types of loading. Lekhnitskii [1] developed the solution for composite cylinder under bending load by using the system of partial differential equations. Kollár and Springer [2] performed a stress analysis on thin to thick-walled composite cylinders under hydrothermal and mechanical loads. Jolicoeur and Cardou [3] developed a general analytical solution in order to find the stresses and displacements fields of a composite cylinder subjected to bending, tensile and torsion loads. Cylinders made of functionally graded materials (FGM) under tension and bending were analysed [4]. An analysis on a cylindrically anisotropic elastic body was made when the body was subjected to extension, torsion, bending and thermo-mechanical [5]. Huang [6] developed the ultimate bending response of a solid composite cylinder reinforced with uniaxially continuous fibers. Fatigue behavior of unidirectional glass fiber reinforced polyester composites under in-phase combined torsion/bending loading was investigated [7]. A formulation of Generalized Beam Theory was derived to analyze the non-classical effects on the structural behavior of FRP composite circular hollow sections [8]. The effects of inner and outer reinforcements on the bending behavior of a thin walled tube were studied [9]. The stress analysis of hollow composite cylindrical structures subjected to different loads was performed [10]. Their method was efficient for thin-walled hollow composite tubes. Based on the nonlinear ring theory, mechanical behavior of thermoplastic tube under combined bending and tension was investigated [11]. They verified formulations with FEM results obtained using ABAQUS. Menshykova and Guz [12] performed a stress analysis on laminated thick composite pipes subjected to bending loading. They found stresses as a function of the material properties, thickness, lay-up and the magnitude of bending load. A model were developed to study the failure of 0° laminated composite tubes under static and fatigue loadings [13]. Wang et al. [14] analyzed the behavior of luffa-filled tubes

* Corresponding author. Tel.: +1 514 848 2424; fax: +1 514 848 3175.
E-mail address: h_yazd@encs.concordia.ca (H. Yazdani Sarvestani).

http://dx.doi.org/10.1016/j.compositesb.2015.10.025
1359-8368/

under uniaxial compression numerically using and analytically using finite element analysis and theoretical models, respectively. In addition, they validated FEA models against experimental data. Gohari et al. [15] used first-ply failure to study a laminated glass fiber reinforced polymer composite shell subjected to internal pressure. Capela et al. [16] investigated the fatigue behaviour of composite tubes under bending/torsion dynamic loadings. Recently, static analysis of carbon nanotube-reinforced composite cylinder under thermo-mechanical was studied using Mori–Tanaka theory [17]. Recently, a method to analyze stress distributions of the composite cantilever straight tube was developed [18].

Although finite element and other methods reviewed above can be used for analysing tube structures, it is necessary to do some actions for each structure every time some dimensions are changed. Therefore, it is desired to have a method where the input for the solution is simple; i.e. one only needs to enter the actual dimensions without meshing work. The present work is devoted to develop an analytical method that can provide stresses, strains and deformations for a thick composite tube subjected to pure bending moment with simple inputs. The layer-wise method, which includes the full three-dimensional constitutive relations, is employed to calculate the three-dimensional stress distributions within the tube. Then, the comparison is made between results obtained using the proposed analytical method, experimental data and FEM (ANSYS). Finally, effects of reinforcing composite tubes with multi-walled carbon nanotubes (MWCNTs) on stress distributions are studied.

2. Theoretical Formulation

2.1. Displacement Field

A thick laminated orthotropic straight tube with mean radius R and thickness h is subjected to bending moment M_0 as shown in Figure 1. The cylindrical coordinates (x, θ, r) are placed at the middle of the composite tube where x and r are the axial and radial coordinate, respectively. The integration of the appropriate linear strain-displacement relations of elasticity, within cylindrical coordinate system will yield the following displacement field for the kth layer:

$$u_1^{(k)}(x,\theta,r) = xr\left(C_5^{(k)}\cos\theta + C_4^{(k)}\sin\theta\right) + C_6^{(k)}x + u^{(k)}(\theta,r) \tag{1a}$$

$$u_2^{(k)}(x,\theta,r) = x\left(C_1^{(k)}\cos\theta - C_2^{(k)}\sin\theta - C_3^{(k)}r\right) - \frac{1}{2}x^2\left(C_4^{(k)}\cos\theta - C_5^{(k)}\sin\theta\right) + v^{(k)}(\theta,r) \tag{1b}$$

$$u_3^{(k)}(x,\theta,r) = x\left(C_1^{(k)}\sin\theta + C_2^{(k)}\cos\theta\right) - \frac{1}{2}x^2\left(C_5^{(k)}\cos\theta + C_4^{(k)}\sin\theta\right) + w^{(k)}(\theta,r) \tag{1c}$$

where $u_1^{(k)}(x,\theta,r)$, $u_2^{(k)}(x,\theta,r)$ and $u_3^{(k)}(x,\theta,r)$ represent the displacement components in the x, θ and r directions, respectively, of a material point located at (x, θ, r) in the kth ply of the laminated composite tube in Figure 1. Also, $u^{(k)}(\theta,r)$, $v^{(k)}(\theta,r)$ and $w^{(k)}(\theta,r)$ (k=1, 2, …, N+1) represent the displacement components of all points located on the kth layer in the undeformed laminated tube. In order to satisfy the interfacial continuities of the displacement components, it is necessary that the integration constants appearing in Eqs. (1) to be the same for all layers. Thus, Eqs. (1) are represented as:

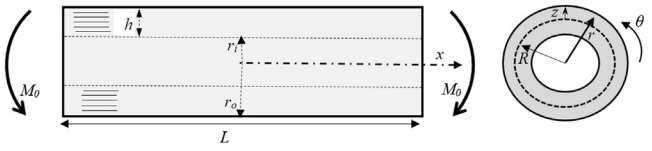

Figure 1. The geometry of a composite straight tube and the coordinate system.

$$u_1^{(k)}(x,\theta,r) = xr(C_5\cos\theta + C_4\sin\theta) + C_6x + u^{(k)}(\theta,r) \tag{2a}$$

$$u_2^{(k)}(x,\theta,r) = x(C_1\cos\theta - C_2\sin\theta - C_3r) - \frac{1}{2}x^2(C_4\cos\theta - C_5\sin\theta) + v^{(k)}(\theta,r) \tag{2b}$$

$$u_3^{(k)}(x,\theta,r) = x(C_1in\theta + C_2\cos\theta) - \frac{1}{2}x^2(C_5\cos\theta + C_4\sin\theta) + w^{(k)}(\theta,r) \tag{2c}$$

Moreover, in Eq. (2a), $u^{(k)}(\theta,r)$ can be replaced by $-C_1r\sin\theta + u^{(k)}(\theta,r)$. It can be shown that the terms involving C_1 in Eq. (2) correspond to an infinitesimal rigid-body rotation. These terms will, therefore, be ignored in the following developments since they will not generate any strain. Similarly, it can be readily shown that the terms involving C_2 must also be eliminated since they represent another rigid-body rotation of the tube. Furthermore, as long as the loading conditions at the two ends of the tube are identical, the constant C_4 must vanish in order to satisfy the symmetry condition in deformation $u_3^{(k)}(x,\theta,r) = u_3^{(k)}(-x,-\theta,r)$. It is thus concluded that the most general form of the displacement field for the kth layer of a composite tube is given as:

$$u_1^{(k)}(x,\theta,r) = C_5xr\cos\theta + C_6x + u^{(k)}(\theta,r) \tag{3a}$$

$$u_2^{(k)}(x,\theta,r) = -C_3rx + \frac{1}{2}C_5x^2\sin\theta + v^{(k)}(\theta,r) \tag{3b}$$

$$u_3^{(k)}(x,\theta,r) = -\frac{1}{2}C_5x^2\cos\theta + w^{(k)}(\theta,r) \tag{3c}$$

2.2. Layerwise Theory (LWT)

The equivalent single-layer theories are unable to precisely represent the local phenomena in laminated composites, like stress and strain distributions. But then, the LWTs, which consider real 3-D behavior of each layer, are able to present accurate results considering the localized phenomena. Many investigations on the use of LWT for analyzing composite structures were performed [19, 20]. In LWT, the displacement components of a generic point in the laminate are conveniently given as:

$$u_1(x,\theta,z) = u_i(x,\theta)\Phi_i(z) \tag{4a}$$

$$u_2(x,\theta,z) = v_i(x,\theta)\Phi_i(z) \tag{4b}$$

$$u_3(x,\theta,z) = w_i(x,\theta)\Phi_i(z) \quad (i = 1,2,\ldots,N+1) \tag{4c}$$

where k, here and in what follows, being a dummy index implying summation of terms from i=1 to i=N+1. In Eqs. (4), u_1, u_2 and u_3 denote the displacement components in the x, θ and r directions, respectively. Also, $u_i(x,\theta)$, $v_i(x,\theta)$ and $w_i(x,\theta)$ represent the displacements of the points initially located on the ith surface of the laminated tube in the x, θ and r directions, respectively.

Furthermore, $\Phi_i(z)$ is the global Lagrangian interpolation function that is used for the discretization of the displacement through-thickness and can have linear, quadratic or higher-order polynomial variations of the thickness coordinate z. It is to be noted that the accuracy of LWT can be enhanced by subdividing each physical layer into a finite number of numerical layers. Clearly, as the number of subdivision through-thickness is increased, the number of governing equations and the accuracy of the results are increased. The linear global interpolation function is defined as:

$$\Phi_k(z)=\begin{cases}0 & z\le z_{k-1}\\ \psi^2_{k-1}(z) & z_{k-1}\le z\le z_k\\ \psi^1_k(z) & z_k\le z\le z_{k+1}\\ 0 & z\ge z_{k+1}\end{cases}\quad (k=1,2,\ldots,N+1) \tag{5}$$

where $\psi^j_k(j=1,2)$ represent the local Lagrangian linear interpolation functions within the kth layer which are defined as:

$$\psi^1_k(z)=\frac{1}{h_k}(z_{k+1}-z)\ \text{ and }\ \psi^2_k(z)=\frac{1}{h_k}(z-z_k) \tag{6}$$

where h_k is the thickness of the kth layer. Based on the elasticity displacement field in Eqs. (3), the LWT displacement field in Eqs. (4) is rewritten as:

$$u^{(k)}_1(x,\theta,z)=C_5x(R+z)\cos\theta+C_6x+U_k(\theta)\Phi_k(z) \tag{7a}$$

$$u^{(k)}_2(x,\theta,z)=-C_3(R+z)x+\frac{1}{2}C_5x^2\sin\theta+V_k(\theta)\Phi_k(z) \tag{7b}$$

$$u^{(k)}_3(x,\theta,z)=-\frac{1}{2}C_5x^2\cos\theta+W_k(\theta)\Phi_k(z) \tag{7c}$$

By introducing $r=R+z$ (*see Figure 1*), the strain–displacement relations are as given as:

$$\varepsilon_x=\frac{\partial u_1}{\partial x},\quad \varepsilon_\theta=\frac{1}{R+z}\frac{\partial u_2}{\partial\theta}+\frac{u_3}{R+z},\quad \gamma_{x\theta}=\frac{\partial u_2}{\partial x}+\frac{1}{R+z}\frac{\partial u_1}{\partial\theta}$$
$$\gamma_{\theta z}=\frac{1}{R+z}\frac{\partial u_3}{\partial\theta}+\frac{\partial u_2}{\partial z}-\frac{u_2}{R+z},\quad \gamma_{xz}=\frac{\partial u_3}{\partial x}+\frac{\partial u_1}{\partial z},\quad \varepsilon_z=\frac{\partial u_3}{\partial z} \tag{8}$$

Substitution of Eqs. (7) into the strain–displacement relations (8) yields the following results:

$$\varepsilon_x=(R+z)(C_5\cos\theta+C_4\sin\theta)+C_6,\quad \varepsilon_\theta=\frac{V'_k+W_k}{R+z}\Phi_k,\quad \varepsilon_z=W_k\Phi'_k$$
$$\gamma_{\theta z}=\frac{W'_k-V_k}{R+z}\Phi_k+V_k\Phi'_k,\quad \gamma_{xz}=U_k\Phi'_k+(C_1\sin\theta+C_2\cos\theta),$$
$$\gamma_{x\theta}=(C_1\cos\theta-C_2\sin\theta-C_3(R+z))+\frac{U'_k\Phi_k}{R+z} \tag{9}$$

In Eq. (9) and what follows, a prime indicates an ordinary differentiation with respect to an appropriate variable (i.e., either θ or z). The equilibrium equations of a composite straight tube with N numerical layers are obtained by employing Eq. (9) in the principle of minimum total potential energy [21]. The results are, in general, $3(N+1)$ local equilibrium equations corresponding to $3(N+1)$ unknown functions U_k, V_k, and W_k and three global equilibrium equations associated with the three parameters C_3, C_5 and C_6. According to the principle of minimum total potential energy at the equilibrium condition of a body the variation of the total potential energy Π of the body must vanish which consists of:

$$\delta\,\Pi\equiv\delta U+\delta V=0 \tag{10}$$

where δU is the variation of total strain energy of the body as follows:

$$\delta U=\int_{-a}^{a}\int_{-h/2}^{h/2}\int_{-\pi}^{\pi}(\sigma_x\delta\varepsilon_x+\sigma_\theta\delta\varepsilon_\theta+\sigma_z\delta\varepsilon_z+\sigma_{\theta z}\delta\gamma_{\theta z}+\sigma_{xz}\delta\gamma_{xz}+\sigma_{x\theta}\delta\gamma_{x\theta})\mathrm{d}\theta\mathrm{d}z\mathrm{d}x \tag{11}$$

In Eq. (10), V is negative of the work done on the body by the specified external forces. It is written that, $V=-2M_0\cdot\frac{u_1(x=\pm a,\theta,z)}{r}=-2M_0C_5a\cos\theta$ and therefore, $\delta V=-2M_0\delta C_5a\cos\theta$. Also, the variations of strains in Eq. (9) are found as:

$$\delta\varepsilon_x=\delta C_5(R+z)\cos\theta+\delta C_6,\quad \delta\varepsilon_\theta=\left(\delta V'_k+\delta W_k\right)\frac{\Phi_k}{R+z},\quad \delta\varepsilon_z=\delta W_k\Phi'_k$$
$$\delta\gamma_{\theta z}=\left(\delta W'_k-\delta V_k\right)\frac{\Phi_k}{R+z}+\delta V_k\Phi'_k,\quad \delta\gamma_{xz}=\delta U_k\Phi'_k,$$
$$\delta\gamma_{x\theta}=-\delta C_3(R+z)+\delta U'_k\frac{\Phi_k}{R+z} \tag{12}$$

Employing the fundamental lemma of calculus of variations, the equilibrium equations and the associated boundary conditions of a laminated tube under pure bending are obtained as:

$$\delta U_k:\ Q^k_x-\frac{dM^k_{x\theta}}{d\theta}=0 \tag{13a}$$

$$\delta V_k:\ Q^k_\theta-\frac{dM^k_\theta}{d\theta}-R^k_\theta=0 \tag{13b}$$

$$\delta W_k:\ M^k_\theta-\frac{dR^k_\theta}{d\theta}+N^k_z=0 \tag{13c}$$

$$\delta C_3:\ \int_{-\pi}^{\pi}\int_{-h/2}^{h/2}\sigma_{x\theta}(R+z)^2dzd\theta=0 \tag{14a}$$

$$\delta C_5:\ \int_{-\pi}^{\pi}\int_{-h/2}^{h/2}\sigma_x(R+z)^2\cos\theta dzd\theta=M_0 \tag{14b}$$

$$\delta C_6:\ \int_{-\pi}^{\pi}\int_{-h/2}^{h/2}R\sigma_xdzd\theta=0 \tag{14c}$$

where M_0 represents the prescribed value of bending moment applied at both ends of the composite tube. The generalized stress and moment resultants are defined as:

$$\left(N^k_z,Q^k_x,Q^k_\theta\right)=\int_{-h/2}^{h/2}(\sigma_z,\sigma_{xz},\sigma_{\theta z})\,\Phi'_k\,dz \tag{15a}$$

$$\left(M^k_\theta,M^k_{x\theta},R^k_\theta\right)=\int_{-h/2}^{h/2}\frac{1}{R+z}(\sigma_\theta,\sigma_{x\theta},\sigma_{\theta z})\,\Phi_k\,dz \tag{15b}$$

It is to be noted that in Eqs. (13) and Eqs. (15), the superscript k

refers to the kth layer in the laminated composite tube. Also, the following traction-free boundary conditions must be satisfied:

$$R_\theta^k = Q_x^k = N_z^k = 0 \quad (at\ z = \pm h/2) \tag{16}$$

The three-dimensional constitutive law within the kth layer of laminate is given as follow [22]:

$$\begin{pmatrix} \sigma_x \\ \sigma_\theta \\ \sigma_z \\ \sigma_{\theta z} \\ \sigma_{xz} \\ \sigma_{x\theta} \end{pmatrix}^{(k)} = \begin{bmatrix} \overline{C}_{11} & \overline{C}_{12} & \overline{C}_{13} & 0 & 0 & \overline{C}_{16} \\ \overline{C}_{12} & \overline{C}_{22} & \overline{C}_{23} & 0 & 0 & \overline{C}_{26} \\ \overline{C}_{13} & \overline{C}_{23} & \overline{C}_{33} & 0 & 0 & \overline{C}_{36} \\ 0 & 0 & 0 & \overline{C}_{44} & \overline{C}_{45} & 0 \\ 0 & 0 & 0 & \overline{C}_{45} & \overline{C}_{55} & 0 \\ \overline{C}_{16} & \overline{C}_{26} & \overline{C}_{36} & 0 & 0 & \overline{C}_{66} \end{bmatrix}^{(k)} \begin{pmatrix} \varepsilon_x \\ \varepsilon_\theta \\ \varepsilon_z \\ \gamma_{\theta z} \\ \gamma_{xz} \\ \gamma_{x\theta} \end{pmatrix}^{(k)} \tag{17}$$

where $\overline{C}_{ij}^{(k)}$ represent the off-axis stiffnesses. By substituting Eq. (12) into Eq. (17) and the subsequent results into Eqs. (15), the stress resultants are given the following relations:
where the laminate rigidities in Eq. (18) are defined as:

$$\begin{aligned} \left(A_{pq}^{kj}, \overline{B}_{pq}^{kj}, D_{pq}^{kj}\right) &= \sum_{i=1}^{N} \int_{z_i}^{z_{i+1}} \overline{C}_{pq}^{(i)} \left(\Phi_k' \Phi_j', \Phi_k \Phi_j', \Phi_k \Phi_j\right) \mathrm{d}z \\ \left(B_{pq}^{kj}, H_{pq}^{kj}, G_{pq}^{kj}\right) &= \sum_{i=1}^{N} \int_{z_i}^{z_{i+1}} \overline{C}_{pq}^{(i)} \left(\frac{\Phi_k \Phi_j'}{R+z}, \frac{\Phi_k \Phi_j'}{(R+z)^2}, \frac{\Phi_k \Phi_j}{R+z}\right) \mathrm{d}z \\ \left(A_{pq}^{k}, B_{pq}^{k}, \overline{B}_{pq}^{k}\right) &= \sum_{i=1}^{N} \int_{z_i}^{z_{i+1}} \overline{C}_{pq}^{(i)} \left(\Phi_k', \Phi_k, \Phi_k'(R+z)\right) \mathrm{d}z \\ \left(D_{pq}^{k}, F_{pq}^{k}, E_{pq}^{k}\right) &= \sum_{i=1}^{N} \int_{z_i}^{z_{i+1}} \overline{C}_{pq}^{(i)} \left(\frac{\Phi_k}{(R+z)^2}, \frac{\Phi_k}{R+z}, \frac{\Phi_k'}{R+z}\right) \mathrm{d}z \\ & (k, j = 1, 2, \ldots, N+1) \end{aligned} \tag{19}$$

where z direction is thickness coordinate as seen in Figure 1.The local displacement equilibrium equations within the proposed method are obtained by substituting Eq. (18) into Eq. (13):

$$\begin{aligned} \left(N_z^k, M_\theta^k, M_{x\theta}^k\right) &= \left(B_{36}^{jk}, H_{26}^{kj}, H_{66}^{kj}\right) U_j' + \left(B_{23}^{jk}, H_{22}^{kj}, H_{26}^{kj}\right) V_j' + \left(B_{23}^{jk} + \overline{B}_{33}^{kj}, H_{22}^{kj}, H_{26}^{kj}\right) W_j - \left(\overline{B}_{36}^{k}, B_{26}^{k}, B_{66}^{k}\right) C_3 + \left(\overline{B}_{13}^{k}, B_{12}^{k}, B_{16}^{k}\right) C_5 \cos\theta \\ &\quad + \left(A_{13}^{k}, F_{12}^{k}, F_{16}^{k}\right) C_6 \\ \left(Q_x^k, Q_\theta^k, R_\theta^k\right) &= \left(A_{55}^{kj}, A_{45}^{kj}, B_{45}^{kj}\right) U_j + \left(A_{45}^{kj} - B_{45}^{jk}, A_{44}^{kj} - B_{44}^{jk}, B_{44}^{kj} - H_{44}^{kj}\right) V_j + \left(B_{45}^{jk}, B_{44}^{jk}, H_{44}^{kj}\right) W_j' \end{aligned} \tag{18}$$

$$\begin{aligned} &\delta U_k : -H_{66}^{kj} U_j'' + A_{55}^{kj} U_j - H_{26}^{kj} V_j'' - B_{45}^{jk} V_j - \left(H_{26}^{kj} + G_{36}^{kj} - B_{45}^{jk}\right) W_j' = -B_{16}^{k} C_5 \sin\theta \\ &\delta V_k : -H_{26}^{kj} U_j'' + \left(A_{45}^{kj} - B_{45}^{kj}\right) U_j - H_{22}^{kj} V_j'' + \left(A_{44}^{kj} - B_{44}^{kj} - B_{44}^{jk} + H_{44}^{kj}\right) V_j - \left(H_{22}^{kj} + G_{23}^{kj} - B_{44}^{jk} + H_{44}^{kj}\right) W_j' = -B_{12}^{k} C_5 \sin\theta \\ &\delta W_k : \left(-B_{45}^{kj} + H_{26}^{kj} + B_{36}^{jk}\right) U_j' + \left(H_{44}^{kj} - B_{44}^{kj} + H_{22}^{kj} + B_{23}^{jk}\right) V_j' - H_{44}^{kj} W_j'' + \left(H_{22}^{kj} + B_{23}^{jk} + G_{23}^{kj} + \overline{B}_{33}^{kj}\right) W_j = \left(\overline{B}_{36}^{k} + B_{26}^{k}\right) C_3 \\ &\qquad - \left(\overline{B}_{13}^{k} + B_{12}^{k}\right) C_5 \cos\theta - \left(A_{13}^{k} + F_{12}^{k}\right) C_6 \\ &k = 1, 2, \ldots, N+1 \end{aligned} \tag{20}$$

Also, the global equilibrium equations of the composite tube are expressed in terms of displacement functions by substituting Eq. (9) into Eqs. (17) and the subsequent results into Eqs. (14). The results are given as:

$$\begin{aligned} &\delta C_3 : \frac{1}{h} \int_{-\pi}^{\pi} \left(\overline{B}_{16} C_6 + \overline{D}_{16} C_5 \cos\theta + B_{26}^{k}\left(V_j' + W_j\right) + \overline{B}_{36}^{k} W_j - \overline{D}_{66} C_3 + A_{66}^{k} U_j'\right) d\theta = 0 \\ &\delta C_5 : \int_{-\pi}^{\pi} \begin{pmatrix} \overline{B}_{11} C_6 \cos\theta + \overline{D}_{11} C_5 \cos^2\theta + B_{12}^{k}\left(V_j' + W_j\right)\cos\theta + F_{13}^{k} W_j \cos\theta \\ -\overline{D}_{16} C_3 \cos\theta + B_{16}^{k} U_j' \cos\theta \end{pmatrix} d\theta = M_0 \\ &\delta C_6 : \int_{-\pi}^{\pi} \left(\overline{A}_{11} C_6 + \overline{B}_{11} C_5 \cos\theta + F_{12}^{k}\left(V_j' + W_j\right) + B_{13}^{k} W_j - \overline{B}_{16} C_3 + F_{16}^{k} U_j'\right) d\theta = 0 \end{aligned} \tag{21}$$

where the extra laminate rigidities appearing in Eqs. (21) are written as:

$$\left(\overline{A}_{pq}, \overline{B}_{pq}, \overline{D}_{pq}\right) = \sum_{i=1}^{N} \int_{z_i}^{z_{i+1}} \overline{C}_{pq}^{(i)} \left(1, R+z, (R+z)^2\right) \mathrm{d}z \tag{22}$$

3. Analytical Solution

The system in Eqs. (20) shows *3(N+1)* coupled ordinary differential equations with constant coefficients which may be displayed in a matrix form as follows:

$$[M]\left\{\eta''\right\} + [K]\{\eta\} = \{F\}\{C\} \tag{23}$$

where

$$\begin{aligned} &\{\eta\} = \left\{\{U\}^T, \{V\}^T, \{\overline{W}\}^T\right\}^T \\ &\{U\} = \{U_1, U_2, ..., U_{N+1}\}^T \quad \{C\} = \{C_3, C_5, C_6\}^T \\ &\{V\} = \{V_1, V_2, ..., V_{N+1}\}^T \\ &\{\overline{W}\} = \{\overline{W}_1, \overline{W}_2, ..., \overline{W}_{N+1}\}^T \end{aligned} \tag{24a}$$

and

$$\overline{W}_j = \int^{\theta} W_j \mathrm{d}\theta \tag{24b}$$

The coefficient matrices [M], [K] and [F] in Eq. (23) are defined in the Appendix. It can readily be confirmed that the general solution of Eq. (23) may be presented as:

$$\{\eta\} = [\psi][\sinh(\lambda\theta)]\{k\} + [K]^{-1}\{F\}\{C\} \tag{25}$$

and [sinh (λθ)] is a *3(N+1)×3(N+1)* diagonal matrix. That is:

$$[\sinh(\lambda\theta)] = diag\left(\sinh(\lambda_1\theta), \sinh(\lambda_2\theta), ..., \sinh\left(\lambda_{3(N+1)}\theta\right)\right) \tag{26}$$

Also [ψ] and $(\lambda_1^2, \lambda_2^2, \ldots, \lambda_{3(N+1)}^2)$ are the model matrix and eigenvalues of $(-[M]^{-1}[K])$, respectively. Matrix {k} is an unknown vector representing *3(N+1)* integration constants. The constants *Cj* (j=3, 5, 6) must be calculated within LWT analysis. Therefore, the boundary conditions in Eq. (16) are first imposed to analytically obtain the vector {k} in terms of the unknown parameters *Cj* (j=3, 5, 6). These constants are then derived in terms of the specified bending moment M_0 by the satisfaction of the global equilibrium conditions in Eqs. (21).

4. FEM Analysis

The pure bending analysis on the whole composite tube is simulated by finite element method using ANSYS. Stress distributions are also generated to compare with the numerical results obtained using the proposed method. The element used to perform the analysis was the layered solid element, SOLID 185. SOLID 185 is a 3D element which is characterized by 8 nodes and each node has three degree of freedoms. This element can be utilized to model both homogeneous and layered solids. For layered solids such as the considered composite tube, a section should be defined and associated with elements in order to define the number of layers per element, layers thickness, material properties of each layer and layers orientation. The properties of the composite tube are given in Table 2. The composite tube are modeled according to the manufactured tube. The mesh-independency study is done for ANSYS. Mesh refining is performed two times while the element aspect ratio was kept constant. It is noted that for the initial mesh, 194400 elements (*90 (Axial) × 240 (circumferential) × 90 (thickness directions)*) are used to model the structure. For the 1st refined mesh, the thickness and circumferential directions are refined twice as much as initial mesh (*777600 elements totally*). In addition, for the 2nd refined mesh, the axial and circumferential directions are refined twice as much as initial mesh and the thickness direction is refined 4 times as much as initial mesh to model the tube (*3110400 elements totally*). An example is presented to show the stress analysis of composite tube using ANSYS 14.5 (*see Figure 2*).

5. Results and Discussion

In this work, numerical results are presented in four sections. First, the comparison is made between the experimental data and those obtained using the presented method. Then, the numerical results obtained by the proposed method with FEM results are compared. In the section 5.3, the advantages of the proposed method over FEM and other methods are discussed. Finally, effects of using MWCNT in composites on stress distributions of composite straight tubes subjected to pure bending moment are studied. The mechanical properties of the composite tube are given in Table 1 [23].

Furthermore, the stress and strain components are normalized as $\overline{\sigma}_{ij} = \sigma_{ij}/\sigma_0$ and $\overline{\varepsilon}_{ij} = \varepsilon_{ij}/\varepsilon_0$, respectively, where $\sigma_0 = (M.r)/(\pi/64^*(OD^4\text{-}ID^4))$ and $\varepsilon_0 = \sigma_0/E_1$ in which the outer diameter *OD* and the inner diameter *ID* of the composite straight tube. In the present case, the tube section has an internal diameter of 38.1 mm and an external diameter of 61.1 mm, i.e. a wall thickness of 11.5 mm. Also, the length of the tube is 557 mm. Thickness was kept constant for all physical layers [25]. It should be emphasized that in the developed method each actual physical layer can be considered as some mathematical layers with *p* being the number of subdivisions introduced in every layer [21]. In order to increase the accuracy of the developed method, each physical ply is assumed to be 12 sublayers (i.e., *p=12*). Note that the loading condition applied to composite tube is considered according to the experimental work done in which the catastrophic failure did not occur.

5.1. Comparison of the Proposed Method with Experimental Data

In this part, the proposed method results are compared with experimental data. The bending behavior of thick-walled composite tubes was investigated experimentally [25]. The $[-25°/25°]_{45}$ thick-walled thermoplastic composite tubes were manufactured using automated fiber placement technique (AFP) and tested using a pure bending test setup. The pure bending test setup was shown to be a superior alternative test compared to the conventional three-point and four-point bending tests in testing composite tubes [25]. The properties of the manufactured composite tube are given

Table 1
Mechanical properties of composites made of glass/epoxy and glass/epoxy/CNT materials [23].

Properties	E_1 (GPa)	E_2=E_3 (GPa)	G_{12}=G_{13}= G_{23} (GPa)	υ_{12}=υ_{13}= υ_{23}
Glass/epoxy	47.2	11.72	4.1	0.28
Glass/epoxy/0.3 wt% MWCNTs	49.4	12.4	4.22	0.28

Table 2
Mechanical properties of the manufactured composite tube [25].

Properties	E_1 (GPa)	$E_2=E_3$ (GPa)	$G_{12}=G_{13}$ (GPa)	G_{23} (GPa)	$\upsilon_{12}=\upsilon_{13}$	υ_{23}
Carbon AS4/PEEK	115	10	5	3	0.329	0.49

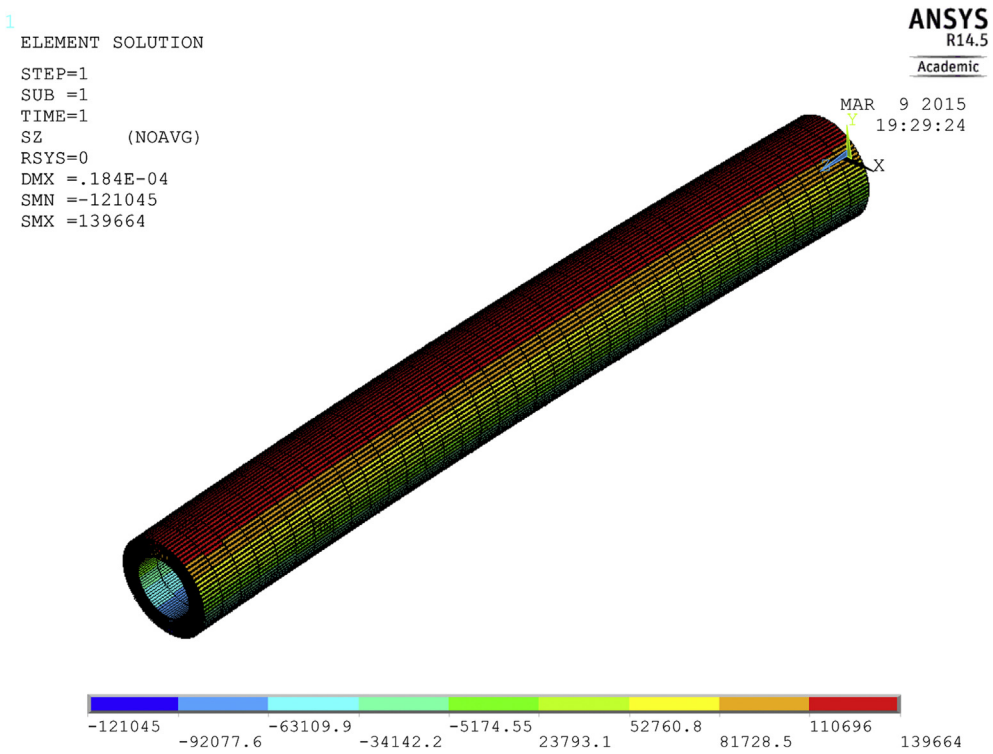

Figure 2. Distribution of axial stress in glass/epoxy/CNT composite tube subjected to pure bending moment using ANSYS 14.5.

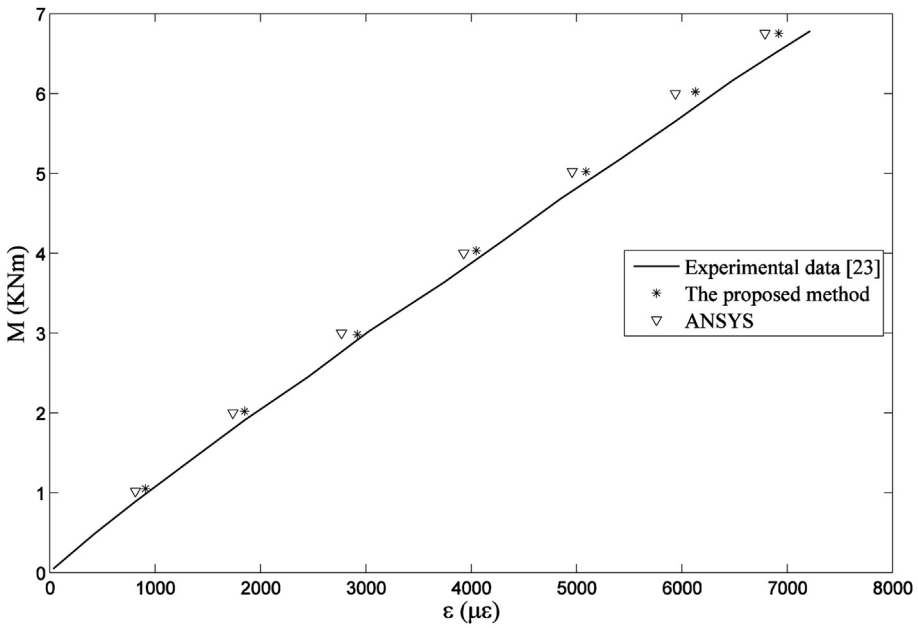

Figure 3. Applied moment-axial strain at the top line of the tube (θ=90°).

in Table 2. In the experimental case, the tube section has an internal diameter of 38.1 mm and an external diameter of 61.1 mm. The composite tube was made with 90 layers.

In the experimental investigation [25], the strain gage was bonded on the surface of the composite tube at the top line of the tube (θ=90°) to measure strains. The measured strain results are compared with the calculated strain results using the proposed method at θ=90°, while the tube length is 557 mm. Experimental strain results are shown in Figure 3. In Figure 3, the moment variation versus axial strains is shown. Good agreement is obtained between the analytical analysis and experimental results. In addition, FEM (ANSYS) (*see Figure 3*) is used to evaluate the accuracy of the proposed method. It is seen that the proposed method results are closer to the experimental data than those of FEM (ANSYS). Also, with increasing applied moment, the presented method is more accurate than FEM. It is noted that the 2nd refined mesh (*see section 5.2*) used to get FEM results here.

5.2. Comparison of the Proposed Method and FEM

The radial stress, σ_{zz}, at the mid radius (*r=24.8 mm, -25°/25° interface*) of the $[-25°/25°]_{45}$ laminated orthotropic straight tube obtained by the present method and FEM (ANSYS) is compared in Figure 4a. Good agreement is observed between analytical analysis and FEM (ANSYS) results. Modeling and analyzing of the composite straight tube for initial mesh take around 900 seconds while they take around 1800 and 3500 seconds for the 1st refined and the 2nd refined meshes, respectively. But the modeling and analyzing of the same structure (*same complex lay-up*) using the developed method takes 420 seconds (with using *p=12* in the proposed method). In

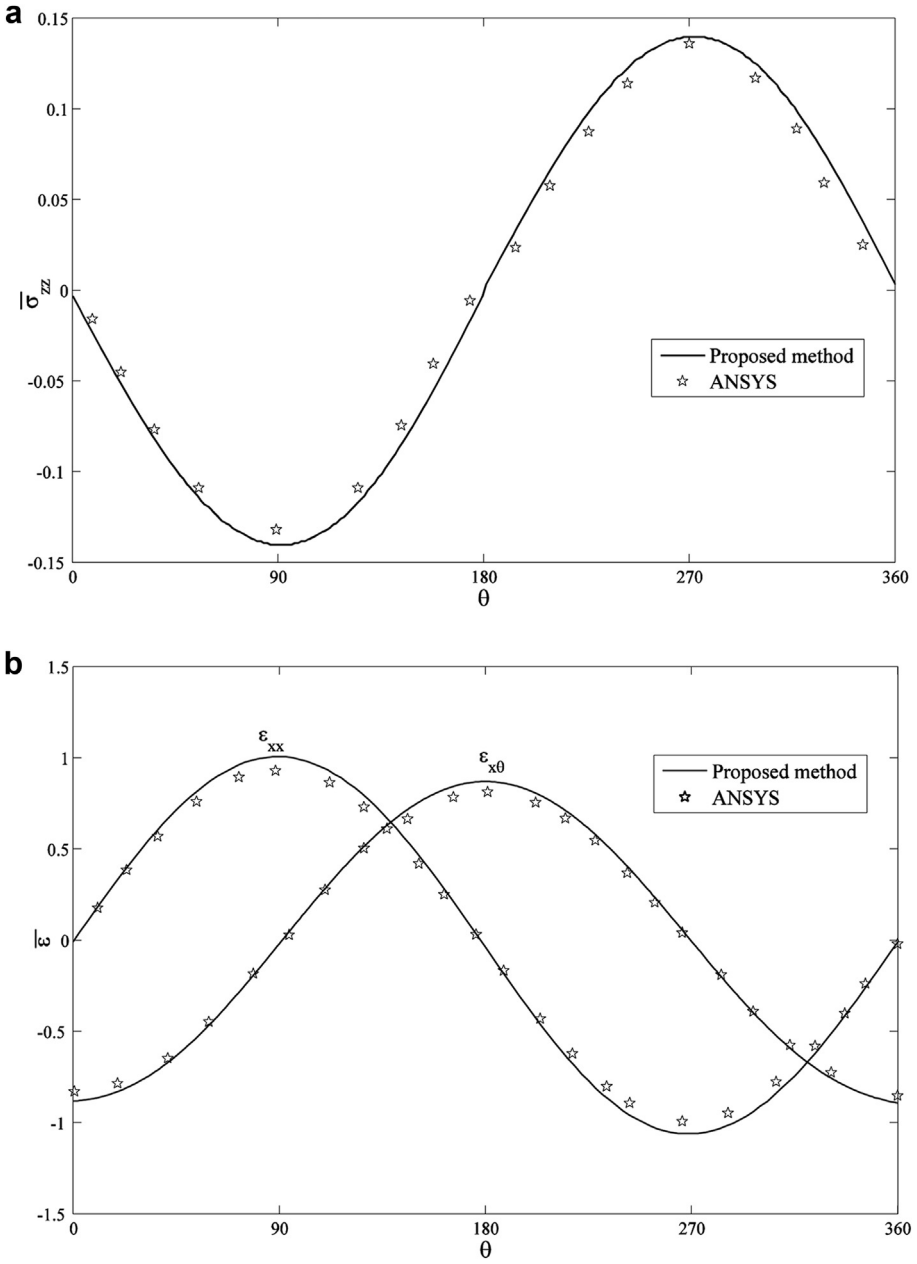

Figure 4. 4a: Comparison of radial stress obtained from the proposed method and ANSYS at the mid radius of the $[-25°/25°]_{45}$ laminated straight tube. 4b: Comparison of axial and shear strains obtained from the proposed method and ANSYS at the mid radius of the $[-25°/25°]_{45}$ laminated straight tube.

addition, distributions of the axial and shear strains, ε_{xx}, $\varepsilon_{x\theta}$, at the at the mid radius (*r=24.8 mm, -25°/25° interface*) of the $[-25°/25°]_{45}$ laminated orthotropic straight tube obtained by the present method and FEM (ANSYS) are compared in Figure 4b. Good agreement is seen again between the proposed method and FEM (ANSYS) results.

5.3. Advantages of the Proposed Method

The most important advantage of the proposed method is that the inputs for the modeling of composite structures with complex lay-up (*see the experimental part lay-up*) are simple, easy to use, and fast to run. Contrary, to model complex lay-up composite structures in FEM, it is necessary to create individual sections and mesh them separately with different lay-up attributes. But, through using the proposed method, it is required to simply input dimensions and lay-ups at the beginning of the program. Therefore, it is obvious that the modeling of orthotropic structures with complex lay-up using FEM (ANSYS) takes much longer than using the developed method. It is noted that the mechanical properties and lay-up sequence are used as inputs for the developed method to analyze laminated composite tubes.

To add to the advantages, high efficiency in terms of computational time is obtained comparing the proposed method with FEM (ANSYS) (*see part 5.1*).

One of the other advantages of the presented method is the accuracy of the obtained results (*see Figure 3*). It was shown that the results obtained using the proposed method is more accurate than FEM results in comparison with experimental data.

In addition, using ANSYS for parametric study is cumbersome while this method can be applied easily for any parametric study with low computational cost. For example, to study the effects of thickness on stress and strain distributions by using FEM (ANSYS), it is necessary to model the geometry for different thicknesses and obviously it takes longer than using the presented method.

The proposed method is developed for analyzing laminated composites tubes made of different types of fibers and polymers in the sense that different mechanical properties can be considered as a result of different types of laminates in the calculations. In addition to above, the proposed method is capable of analyzing composite laminate with different types of tubes with different geometries and loading conditions.

5.4. Effects of Using MWCNT on Stress Distributions

The usefulness of adding MWCNTs in polymer composites was studied [23]. Naghashpour and Hoa [23, 24] improved the mechanical properties of glass fiber/epoxy composites by adding 0.3% wt MWCNTs while enhancing sensing capability of the composites. Here, stress distributions of the composite straight tube subjected to pure bending moment are studied, as well as, effects of adding MWCNTs as reinforcements to composite tubes on the stress distributions. Numerical results obtained using the proposed method at the mid radius (*r=24.8 mm, -25°/25° interface*) are presented.

The distributions of the axial stress, σ_{xx}, and shear stress, $\sigma_{x\theta}$, at the -25°/25° interface of the $[-25°/25°]_{45}$ laminated composite tube along the circumferential direction are shown in Figure 5. It is seen that the axial stress σ_{xx} gives an anti-symmetric behavior while shear stress, $\sigma_{x\theta}$, has the symmetric behavior. In addition, the axial stress, σ_{xx}, is positive at the upper region of tube cross section (0°-180°) while it is negative at the lower region of tube cross section (180°-360°) as it is expected. But, the shear stress, $\sigma_{x\theta}$, is positive at the left region of tube cross section (90°-270°) and it is negative at the right region of tube cross section (270°-360° and 0°-90°). Also, the comparison is made between glass/epoxy/MWCNT composite and glass/epoxy composite tubes. It is observed that the axial stress, σ_{xx}, and shear stress, $\sigma_{x\theta}$, for carbon nanotube-reinforced composite tube are 5% less than those of glass/epoxy composite tube.

The distributions of the interlaminar radial stress, σ_{zz}, and shear stress, σ_{zx}, at the -25°/25° interface of the $[-25°/25°]_{45}$ laminated composite tube along the circumferential direction are shown in Figure 6a. The positive maximum value of the interlaminar normal stress, σ_{zz}, happens at θ=270°. It is noted that the positive radial stress, σ_{zz}, can cause delamination failure in the

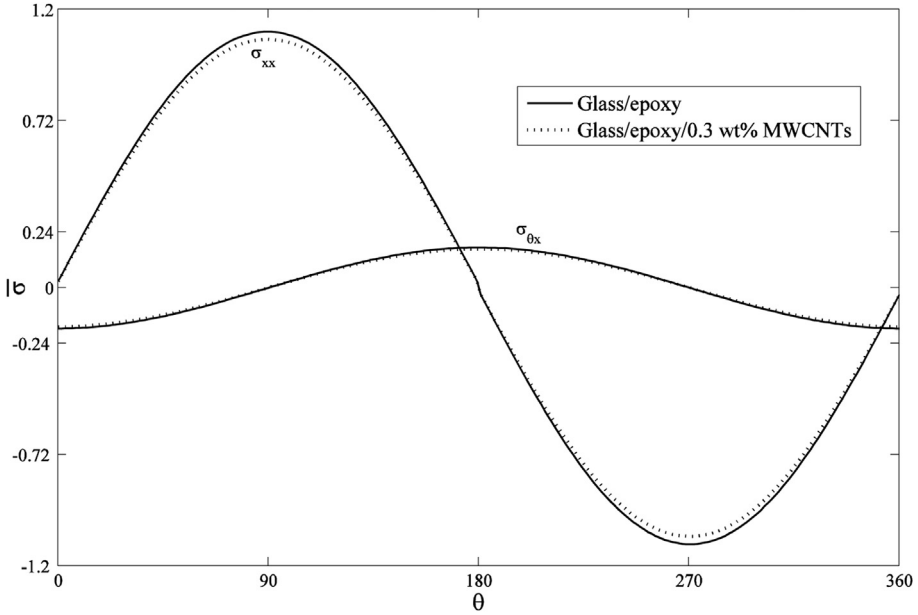

Figure 5. Distributions of the axial stress σ_{xx} and shear stress $\sigma_{x\theta}$ at the mid radius of the $[-25°/25°]_{45}$ laminated composite straight tube made with two different materials.

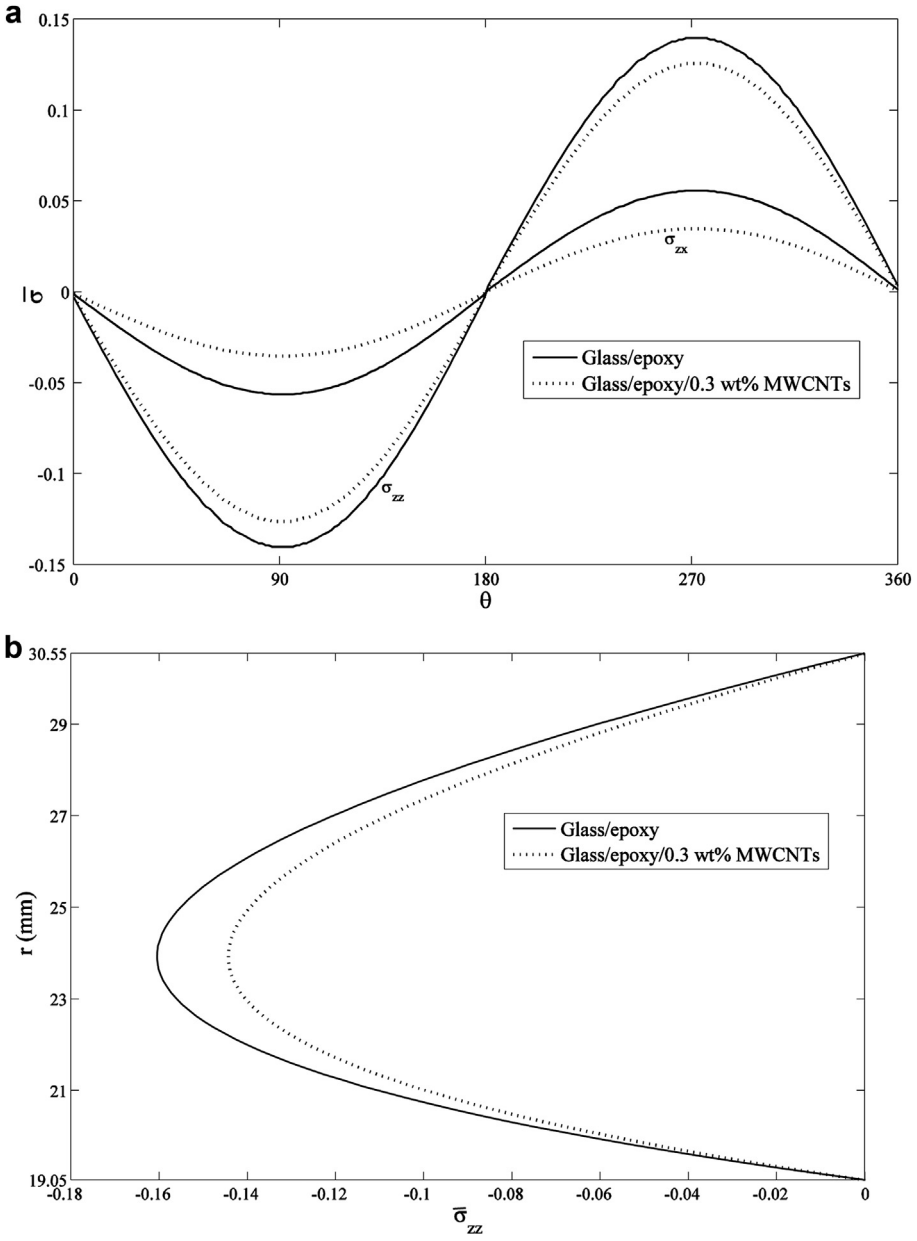

Figure 6. 6a: Distributions of the interlaminar radial stress σ_{zz} and shear stress σ_{zx} at the mid radius of the $[-25^\circ/25^\circ]_{45}$ laminated composite straight tube made with two different materials.6b: Comparison of the interlaminar radial stress σ_{zz} of the $[-25^\circ/25^\circ]_{45}$ laminated composite straight tube made with two different materials at $\theta=90^\circ$ along the tube thickness.

composite tube. Also, it is seen from Figure 6a that composite tube reinforced with MWCNTs, the normal stress σ_{zz}, created between layers of laminated tubes, becomes lower. This may avoid delamination in composite tubes. The magnitude of the interlaminar radial stress, σ_{zz}, is greater than that of the shear stress σ_{zx}. In addition, the shear stress, σ_{zx}, of MWCNT-reinforced composite tube is 10% less than that of glass/epoxy composite tube. Figure 6b shows the comparison of the interlaminar radial stress, σ_{zz}, of the $[-25^\circ/25^\circ]_{45}$ laminated composite straight tube at $\theta=90^\circ$ along the tube thickness. The maximum of radial stress, σ_{zz}, occurs at *r=24 mm* which is *layer 38*. The interlaminar radial stress, σ_{zz}, has the same trend for both composite tubes reinforced with MWCNTs and without MWCNTs.

Figure 7a presents the distributions of the hoop stress, $\sigma_{\theta\theta}$, and shear stress, $\sigma_{\theta z}$, at the -25°/25° interface of the $[-25^\circ/25^\circ]_{45}$ laminated composite tube along the circumferential direction. It is observed that the hoop stress, $\sigma_{\theta\theta}$, is negative at the upper region of the tube cross section while the shear stress, $\sigma_{\theta z}$, sign changes in this region (0°-180°). The maximum value of the hoop stress, $\sigma_{\theta\theta}$, occurs at $\theta=270^\circ$ while maximum value of the shear stress, $\sigma_{\theta z}$, takes place at $\theta=0^\circ$. In addition, it is observed that the hoop and shear stresses of the composite tube reinforced with MWCNTs are 7% less than those of glass/epoxy composite tube. Figure 7b shows the comparison of the hoop stress, $\sigma_{\theta\theta}$, of the $[-25^\circ/25^\circ]_{45}$ laminated composite straight tube at $\theta=90^\circ$ along the tube thickness. It is observed from Figure 7b that the hoop stress, $\sigma_{\theta\theta}$, increases with moving from the inside surface toward the outside surface of the tube for both composite tubes reinforced with MWCNTs and without MWCNTs.

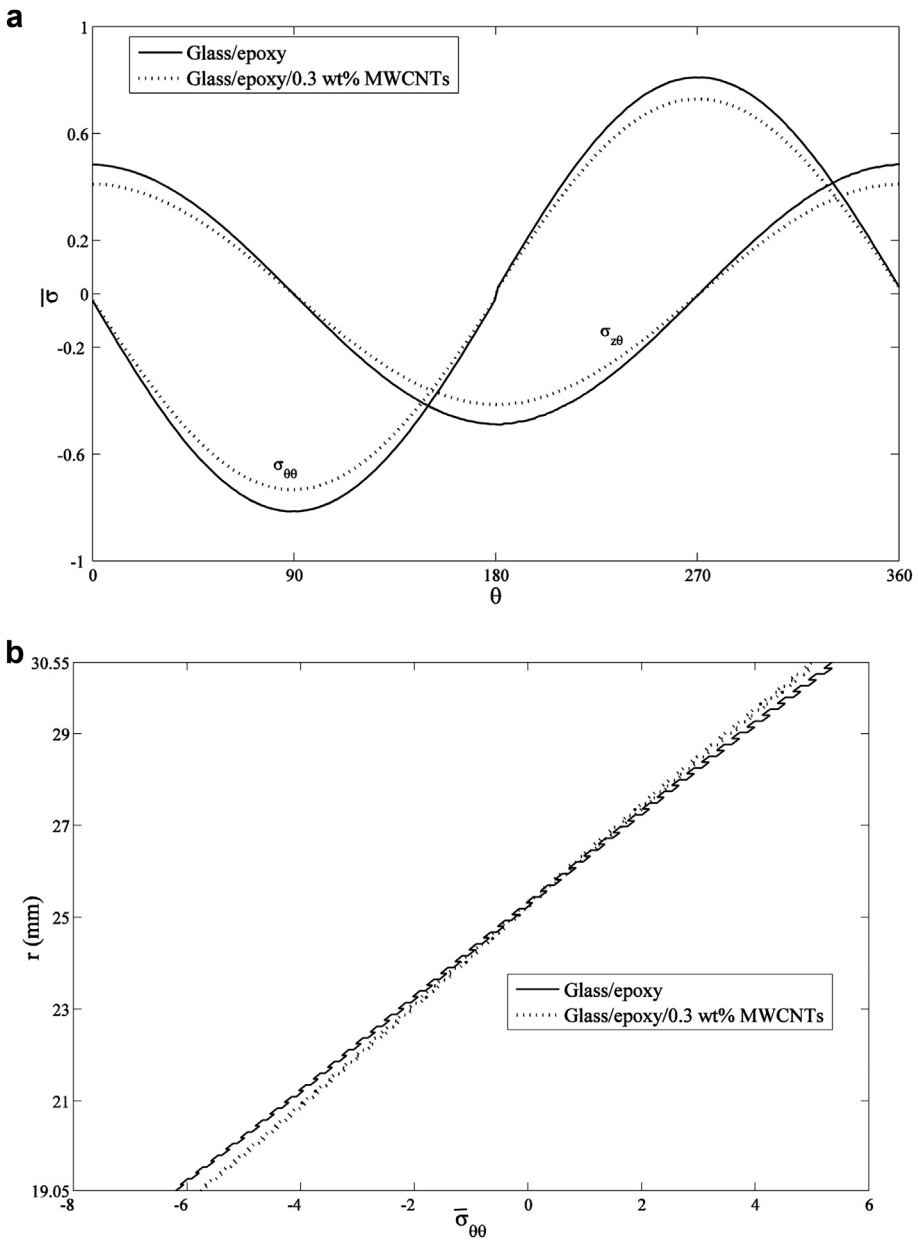

Figure 7. 7a: Distributions of the hoop stress $\sigma_{\theta\theta}$ and shear stress $\sigma_{\theta z}$ at the mid radius of the $[-25^\circ/25^\circ]_{45}$ laminated composite straight tube made with two different materials.7b: Comparison of the hoop stress $\sigma_{\theta\theta}$ of the $[-25^\circ/25^\circ]_{45}$ laminated composite straight tube made with two different materials at $\theta=90^\circ$ along the tube thickness.

The distributions of the interlaminar radial stress, σ_{zz}, and the hoop stress, $\sigma_{\theta\theta}$, of the $[-25^\circ/25^\circ]_{45}$ laminated composite tube along the thickness at $\theta=270^\circ$ are shown in Figure 8. It is noted that the magnitude of the hoop stress, $\sigma_{\theta\theta}$, is greater than that of the radial stress, σ_{zz}, that is why the 0.1 of the hoop stress, $\sigma_{\theta\theta}$, is shown in Figure 8. It is seen that the radial stress, σ_{zz}, is positive totally along the tube thickness while the hoop stress, $\sigma_{\theta\theta}$, is positive and with going to the outside surface of the composite tube is becoming negative. As it is expected from Eqs. (16), it is seen from Figure 8 that the interlaminar radial stress, σ_{zz}, is zero at the inside and outside surfaces of the composite tube ($N_z^k=0$ *at* $z=\pm h/2$). The maximum value of the radial stress, σ_{zz}, occurs before the mid radius along the thickness while the maximum magnitude of the hoop stress, $\sigma_{\theta\theta}$, occurs at the inside surface ($r=$ *19.05 mm*). The hoop stress, $\sigma_{\theta\theta}$, becomes zero somewhere around the mid radius along the thickness.

6. Conclusions

We have proposed the displacement-based method to study the stresses in a thick composite straight tube subjected to pure bending moment. LWT was used to analytically determine the displacement components considering the most general displacement field of elasticity. The equilibrium equations of LWT were subsequently derived through a state-space approach. Moreover, the accuracy of the stresses was studied by comparing the experimental data, numerical results from the proposed method and FEM. Good agreement was found. Furthermore, the presented method was found to be more cost effective and accurate, therefore it was employed to obtain the stresses instead of using FEM (ANSYS). Finally, the numerical results demonstrate that the introduction of CNT in composite tubes makes the stresses to be smaller which gives rise to high performance of composite tubes.

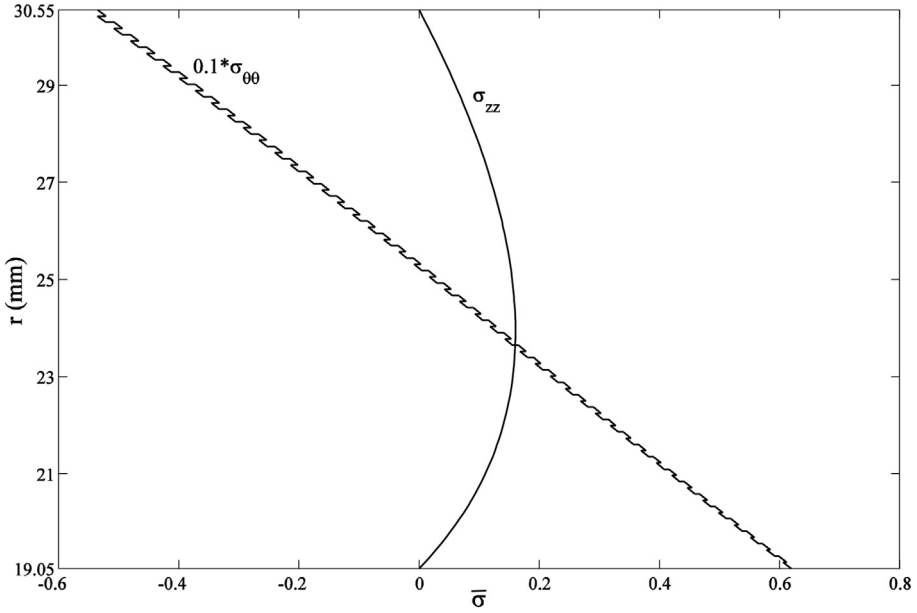

Figure 8. Distributions of the interlaminar radial stress σ_{zz} and hoop stress $\sigma_{\theta\theta}$ of the $[-25^\circ/25^\circ]_{45}$ laminated composite straight tube along the thickness at θ=270°.

Appendix A

The coefficient matrices [M], [K] and [F] in Eq. (23) are obtained as:

$$[M] = \begin{bmatrix} -[H_{66}] & -[H_{26}] & -\left([H_{26}] + [G_{36}] - [B_{45}]^T\right) \\ -[H_{26}] & -[H_{22}] & -\left([H_{22}] + [G_{23}] - [B_{44}]^T + [H_{44}]\right) \\ [0] & [0] & -[H_{44}] \end{bmatrix},$$

$$[K] = \begin{bmatrix} [A_{55}] & -[B_{45}]^T & [0] \\ [A_{45}] - [B_{45}] & [A_{44}] - [B_{44}] - [B_{44}]^T + [H_{44}] & [0] \\ -[B_{45}] + [H_{26}] + [B_{36}]^T & [H_{44}] - [B_{44}] + [H_{22}] + [B_{23}]^T & [H_{22}] + [G_{23}] + [B_{23}]^T + [\bar{B}_{33}] \end{bmatrix},$$

$$\{F\} = \begin{Bmatrix} \{0\} & -\{B_{16}\}\sin\theta & \{0\} \\ \{0\} & -\{B_{12}\}\sin\theta & \{0\} \\ (\{\bar{B}_{36}\} + \{B_{26}\})\theta & -(\{\bar{B}_{13}\} + \{B_{12}\})\sin\theta & -(\{A_{13}\} + \{F_{12}\})\theta \end{Bmatrix}$$

References

[1] Lekhnitskii SG. Theory of elasticity of an anisotropic body. Mir Publisher, Moscow, Russia 1981.
[2] Kollár L, Springer GS. Stress analysis of anisotropic laminated cylinders and cylindrical segments. International Journal of Solids and Structure 1992;29(12):1499–517.
[3] Jolicoeur C, Cardou A. Analytical solution for bending of coaxial orthotropic cylinders. Journal of Engineering Mechanics 1994;120(12):2556–74.
[4] Rooney F, Ferrari M. Tension, bending, and flexure of functionally graded cylinders. International Journal of Solids and Structure 2002;38(3):413–21.
[5] Tarn J. A state space formalism for anisotropic elasticity. Part II: Cylindrical anisotropy. International Journal of Solids and Structure 2002;39(20):5157–72.
[6] Huang ZM. Ultimate strength of a composite cylinder subjected to three-point bending: correlation of beam theory with experiment. Composite Structures 2004;63(3–4):439–45.
[7] El-Assal AM, Khashaba UA. Fatigue analysis of unidirectional GFRP composites under combined bending and torsional loads. Composite Structures 2007;79(4):599–605.
[8] Silvestre N. Non-classical effects in FRP composite tubes. Composites Part B: Engineering 2009;40(8):681–97.
[9] Eksi S, Genel K. Bending response of hybrid composite tubular beams. Thin-Walled Structures 2013;73:329–36.
[10] Sun XS, Tan VBC, Chen Y, Tan LB, Jaiman RK, Tay TE. Stress analysis of multi-layered hollow anisotropic composite cylindrical structures using the homogenization method. Acta Mechanica 2014;225(6):1649–72.
[11] Bai Y, Ruan W, Cheng P, Yu B, Xu W. Buckling of reinforced thermoplastic pipe (RTP) under combined bending and tension. Ships and Offshore Structures 2014;9(5):525–39.
[12] Menshykova M, Guz IA. Stress analysis of layered thick-walled composite pipes subjected to bending loading. International Journal of Mechanical Sciences 2014;88:289–99.
[13] Hochard CH, Miot ST, Thollon Y. Fatigue of laminated composite structures with stress concentrations. Composites Part B: Engineering 2014;65:11–6.
[14] Wang X, Shen J, Zuo ZH, Huang X, Zhou S, Xie YM. Numerical investigation of compressive behavior of luffa-filled tubes. Composites Part B: Engineering 2015;73:149–57.

[15] Gohari S, Sharifi S, Vrcelj Z, Yahya MY. First-ply failure prediction of an unsymmetrical laminated ellipsoidal woven GFRP composite shell with incorporated surface-bounded sensors and internally pressurized. Composites Part B: Engineering 2015;77:502–18.
[16] Capela C, Ferreira JAM, Febra T, Costa JD. Fatigue strength of tubular carbon fibre composites under bending/torsion loading. International Journal of Fatigue 2015;70:216–22.
[17] Arani AG, Haghparast E, Maraghi ZK, Amir S. Static stress analysis of carbon nano-tube reinforced composite (CNTRC) cylinder under non-axisymmetric thermo-mechanical loads and uniform electro-magnetic fields. Composites Part B: Engineering 2015;68:136–45.
[18] Yazdani Sarvestani H, Hoa SV, Hojjati M. Stress Analysis of a Thick Orthotropic Cantilever Tube under Transverse Loading. International Journal of Engineering Science (Submitted).
[19] Yazdani Sarvestani H, Naghashpour A. Investigation of Through-Thickness Stresses in Composite Laminates Using Layerwise Theory. International Journal of Engineering Mathematics 2013;2013:11. Article ID 676743.
[20] Mousanezhad Viyand D, Yazdani Sarvestani H, Nosier A. Stress analysis in symmetric composite laminates subjected to shearing loads. International Journal of Mechanical Sciences 2013;75:16–25.
[21] Reisman H. Elasticity theory and applications. New York: John Wily & Sons, 1980.
[22] Herakovich CT. Mechanics of fibrous composites. New York: John Wiley & Sons, 1998.
[23] Naghashpour A, Hoa SV. In situ monitoring of through-thickness strain in glass fiber/epoxy composite laminates using carbon nanotube sensors. Composites Science and Technology 2013:7841–7.
[24] Naghashpour A, Hoa SV. A technique for real-time detection, location and quantification of damages in large polymer composite structures made of electrically non-conductive fibers and carbon nanotube networks. Journal of Nanotechnology 2013;24:455–502.
[25] El-Geuchy M. reportBending Behavior of Thick-Walled Composite Tubes. PhD Thesis, Concordia University, Montreal, Canada, 2013.